



Pomeron pole plus grey disk model: Real parts, inelastic cross sections and LHC data



S.M. Roy

HBCSE, Tata Institute of Fundamental Research, Mumbai, India

ARTICLE INFO

Article history:

Received 18 June 2016

Received in revised form 2 November 2016

Accepted 15 November 2016

Available online 18 November 2016

Editor: J.-P. Blaizot

ABSTRACT

I propose a two component analytic formula $F(s, t) = F^{(1)}(s, t) + F^{(2)}(s, t)$ for $(ab \rightarrow ab) + (a\bar{b} \rightarrow a\bar{b})$ scattering at energies ≥ 100 GeV, where s, t denote squares of c.m. energy and momentum transfer. It saturates the Froissart–Martin bound and obeys Auberson–Kinoshita–Martin (AKM) [1,2] scaling. I choose $ImF^{(1)}(s, 0) + ImF^{(2)}(s, 0)$ as given by Particle Data Group (PDG) fits [3,4] to total cross sections, corresponding to simple and triple poles in angular momentum plane. The PDG formula is extended to non-zero momentum transfers using partial waves of $ImF^{(1)}$ and $ImF^{(2)}$ motivated by Pomeron pole and ‘grey disk’ amplitudes and constrained by inelastic unitarity. $ReF(s, t)$ is deduced from real analyticity: I prove that $ReF(s, t)/ImF(s, 0) \rightarrow (\pi/\ln s)d/d\tau(\tau ImF(s, t)/ImF(s, 0))$ for $s \rightarrow \infty$ with $\tau = t/(\ln s)^2$ fixed, and apply it to $F^{(2)}$. Using also the forward slope fit by Schegelsky–Ryskin [5], the model gives real parts, differential cross sections for $(-t) < .3$ GeV 2 , and inelastic cross sections in good agreement with data at 546 GeV, 1.8 TeV, 7 TeV and 8 TeV. It predicts for inelastic cross sections for pp or $\bar{p}p$, $\sigma_{inel} = 72.7 \pm 1.0$ mb at 7 TeV and 74.2 ± 1.0 mb at 8 TeV in agreement with pp Totem [7–10] experimental values 73.1 ± 1.3 mb and 74.7 ± 1.7 mb respectively, and with Atlas [12–15] values 71.3 ± 0.9 mb and 71.7 ± 0.7 mb respectively. The predictions $\sigma_{inel} = 48.1 \pm 0.7$ mb at 546 GeV and 58.5 ± 0.8 mb at 1800 GeV also agree with $\bar{p}p$ experimental results of Abe et al. [47] $48.4 \pm .98$ mb at 546 GeV and 60.3 ± 2.4 mb at 1800 GeV. The model yields for $\sqrt{s} > 0.5$ TeV, with PDG2013 [4] total cross sections, and Schegelsky–Ryskin slopes [5] as input, $\sigma_{inel}(s) = 22.6 + .034\ln s + .158(\ln s)^2$ mb, and $\sigma_{inel}/\sigma_{tot} \rightarrow 0.56$, $s \rightarrow \infty$, where s is in GeV 2 units. Continuation to positive t indicates an ‘effective’ t -channel singularity at $\sim (1.5$ GeV) 2 , and suggests that usual Froissart–Martin bounds are quantitatively weak as they only assume absence of singularities upto $4m_\pi^2$.

© 2016 The Author. Published by Elsevier B.V. This is an open access article under the CC BY license (<http://creativecommons.org/licenses/by/4.0/>). Funded by SCOAP³.

1. Introduction

Precision measurements of pp cross sections at LHC [7–16], and in cosmic rays [17] motivate me to present a model for $ab \rightarrow ab$ scattering amplitude at c.m. energies $\sqrt{s} > 100$ GeV described by an analytic formula containing very few parameters. Neglecting terms with a power decrease at high s , the Particle Data Group (PDG) fits to total cross sections [3,4] are the sum of one constant component and another rising as $(\ln s)^2$, corresponding to a simple pole and a triple pole at $J = 1$ in the angular momentum plane,

$$\begin{aligned}\sigma_{tot}^{ab} &= \sigma_{tot}^{(1),ab} + \sigma_{tot}^{(2),ab}, \\ \sigma_{tot}^{(1),ab} &= P^{ab}, \quad \sigma_{tot}^{(2),ab} = H(\ln s/s_M^{ab})^2.\end{aligned}\tag{1}$$

E-mail address: smroy@hbcse.tifr.res.in.

I propose that, analogously, the full amplitude $F(s, t) = F^{(1)}(s, t) + F^{(2)}(s, t)$, where, $F^{(1)}$ is a Pomeron simple pole amplitude, $ImF^{(2)}$ has partial waves with a smooth cut-off at impact parameter $b = R(s)$ corresponding to a grey disk and $ReF^{(2)}(s, t)$ is calculated from a theorem I prove using real analyticity and Auberson–Kinoshita–Martin (AKM) [1,2] scaling for $s \rightarrow \infty$ with fixed $t/(\ln s)^2$. Inelastic unitarity is tested using inputs of total cross sections, forward slopes and Pomeron parameters. Only inputs leading to unitary amplitudes are accepted. Model predictions for inelastic cross sections, near forward real parts and differential cross sections agree with existing data and can be tested against future LHC experiments.

2. Froissart–Martin bound basics

Froissart [18], from the Mandelstam representation, and Martin [19], from axiomatic field theory, proved that the total cross-

section $\sigma_{tot}(s)$ for two particles a, b to go to anything must obey the bound,

$$\sigma_{tot}(s) \leq_{s \rightarrow \infty} C [\ln(s/s_0)]^2, \quad (2)$$

where C, s_0 are unknown constants. It was proved later [20] that $C = 4\pi/(t_0)$, where t_0 is the lowest singularity in the t -channel. This bound has been extremely useful in theoretical investigations [21,22] and high energy models [23–32]. Analogous bounds on the inelastic cross section have been obtained by Martin [33] and Wu et al. [34]; for pion–pion case, Martin and Roy obtained bounds on energy averaged total [35] and inelastic cross sections [36] which also fix the scale factor s_0 in these bounds.

3. Normalization

For the $ab \rightarrow ab$ scattering amplitude $F(s, t)$, $a \neq b$, with k = c.m. momentum, and $z = 1 + t/(2k^2)$,

$$\begin{aligned} F(s, t) &= \sqrt{s}/(4k) \sum_{l=0}^{\infty} (2l+1) P_l(z) a_l(s), \\ \sigma_{tot}(s) &= 4\pi/(k^2) \sum_{l=0}^{\infty} (2l+1) Ima_l(s) \\ \frac{d\sigma}{dt} &= \frac{\pi}{k^2} \frac{d\sigma}{d\Omega}(s, t) = \frac{\pi}{k^2} \left| 4 \frac{F(s, t)}{\sqrt{s}} \right|^2, \end{aligned} \quad (3)$$

with the inelastic unitarity constraint $Ima_l(s) \geq |a_l(s)|^2$. For identical particles $a = b$, the partial waves $a_l(s) \rightarrow 2a_l(s)$ in the above partial wave expansions for $F(s, t)$, and $\sigma_{tot}(s)$, but the odd partial waves are zero. We have the same formulae for the unitarity constraint, and the differential cross section as given above.

At high energy, using $a_l(s) \equiv a(b, s)$, $l = bk$, where b is the impact parameter, and $P_l(\cos\theta) \sim J_0((2l+1)\sin(\theta/2)) + O(\sin^2(\theta/2))$, we have the impact parameter representation,

$$\begin{aligned} F(s, t) &= k\sqrt{s}/2 \int_0^\infty b db a(b, s) J_0(b\sqrt{-t}) \\ \sigma_{tot} &= 8\pi \int_0^\infty b db Ima(b, s); \quad \sigma_{el} = 8\pi \int_0^\infty b db |a(b, s)|^2 \\ d\sigma/dt &= 4\pi \left| \int_0^\infty b db a(b, s) J_0(b\sqrt{-t}) \right|^2. \end{aligned} \quad (4)$$

There exist very good fits to high energy data [37,38] with a very large number of free parameters. There are also very good eikonal based models involving several free parameters [23–32]. The recent eikonal based model of Block and Halzen (BH) [39,40] uses high energy data to guess the glue-ball mass and to probe whether the proton is a black disk.

4. A two component partial wave model

I present a two component model with very few parameters and with analytic formulae for the total amplitude incorporating unitarity-analyticity constraints, PDG total cross sections and the AKM scaling theorem.

4.1. Imaginary parts

I use the two component PDG total cross section fit. I propose that in the impact parameter picture, the Imaginary part

$Ima(b, s)$ of the partial waves at fixed s is also a sum of two components, one part $Ima^{(1)}(b, s)$ a Gaussian corresponding to a Pomeron pole, and the other $Ima^{(2)}(b, s)$ a polynomial of degree $2n$ in b^2 with a smooth cut-off at $b = R(s)$, n being a positive integer, so that $Ima^{(2)}(b, s)$ is continuous and has continuous derivative at $b = R(s)$. The second component corresponds to a “grey” disk with cross section rising as $(\ln s)^2$,

$$\begin{aligned} Ima(b, s) &= Ima^{(1)}(b, s) + Ima^{(2)}(b, s), \\ Ima^{(1)}(b, s) &= C(s) \exp(-2b^2/D^2(s)), \\ Ima^{(2)}(b, s) &= E(s)(1 - b^2/R^2(s))^{2n}\theta(R(s) - b), \end{aligned} \quad (5)$$

where $\theta(x) = 1$, for $x \geq 0$, and 0 otherwise. The unitarity constraints are,

$$C(s) \geq 0, \quad E(s) \geq 0, \quad 0 \leq C(s) + E(s) \leq 1. \quad (6)$$

In Eq. (5) we take the simplest choice $n = 1$ in this paper. Using the ansatz for $Ima^{(1)}(b, s)$, integrating over b , and matching the result for $ImF^{(1)}(s, t)$ with the standard small t Pomeron amplitude,

$$F^{(1)}(s, t) = \frac{k\sqrt{s}}{16\pi} \sigma_{tot}^{(1)} \exp(tb_P + t\alpha' \ln s)(i + t\frac{\pi}{2}\alpha'), \quad (7)$$

we obtain,

$$D^2(s) = 8(b_P + \alpha' \ln s), \quad C(s) = \sigma_{tot}^{(1)}/(2\pi D^2(s)). \quad (8)$$

Since $\sigma_{tot}^{(1)}$ is a constant, $C(s) \rightarrow \text{const}/(\ln s)$, $s \rightarrow \infty$ for $\alpha' \neq 0$. Similarly, the ansatz for $Ima^{(2)}(b, s)$ with $n = 1$ yields,

$$ImF^{(2)}(s, t) = E(s) \frac{4k\sqrt{s}}{q^3 R(s)} J_3(qR(s)), \quad q \equiv \sqrt{-t}, \quad (9)$$

where $J_m(x)$ denotes the Bessel function of order m . Hence,

$$\sigma_{tot}^{(2)}(s) = \frac{16\pi}{k\sqrt{s}} ImF^{(2)}(s, 0) = \frac{4\pi}{3} E(s) R^2(s). \quad (10)$$

Thus, $C(s)D^2(s)$ and $E(s)R^2(s)$ are determined from the PDF total cross section fits using Eqs. (8) and (10) respectively. A nice feature of the model is that the above unitarity constraints (6) as well as a stronger version including real parts can be readily tested, and provide acceptability criteria for extrapolations of experimental data for pp scattering.

4.2. Theorem on real parts

Let $F(s, t) = F(y; t)$, $y \equiv ((s-u)/2)^2$ be an $s-u$ symmetric amplitude, with asymptotic behaviour $|s|(\ln|s|)^\gamma |\phi(\tau)|$, $\tau \equiv t(\ln|s/s_0|)^\beta$, where $\phi()$ is a real analytic function of its argument and $\phi(0) = 1$. For fixed physical t , F is real analytic in the cut- y plane with only a right-hand cut from $(2m_a m_b + t/2)^2$ to ∞ . F must be real for $y = |y| \exp(i\pi)$, i.e. $s \rightarrow |s| \exp(i\pi/2)$, and hence replacing $|s| \rightarrow s \exp(-i\pi/2)$, we have for $s \rightarrow \infty$, τ fixed,

$$\begin{aligned} F(s, t) &\sim -C' s \exp(-i\pi/2) (\ln(s/s_0) - i\pi/2)^\gamma \\ &\times \phi(t(\ln(s/s_0) - i\pi/2)^\beta) \end{aligned} \quad (11)$$

Expanding in powers of $1/\ln s$ at fixed τ we get,

$$\frac{ImF(s, t)}{ImF(s, 0)} \rightarrow \phi(\tau); \quad (12)$$

$$\frac{ReF(s, t)}{ImF(s, 0)} \rightarrow \frac{\pi}{2 \ln(s/s_0)} (\gamma \phi(\tau) + \beta \tau \phi'(\tau)), \quad (13)$$

$$\frac{ReF(s, t)}{s} \rightarrow (\pi/2) \left(\frac{\partial(ImF(s, t)/s)}{\partial(\ln(s/s_0))} \right); \quad (14)$$

$$Rea(b, s) \rightarrow (\pi/2) \frac{\partial(Ima(b, s))}{\partial \ln(s/s_0)}, \quad (15)$$

where, due to linearity, the last two equations also hold for a superposition of terms of the form (11), e.g. $F^{(1)} + F^{(2)}$. Note that, (i) $\text{Re}F(s, 0)/\text{Im}F(s, 0)$ agrees with the Khuri–Kinoshita theorem [41], (ii) the case $\beta = \gamma = 1$ agrees with Martin’s geometrical scaling formula [42,43]. (iii) When $\sigma_{\text{tot}} \sim (\ln s)^2$, $\gamma = \beta = 2$, the AKM theorem and Auberson–Roy theorem [1,2] guarantee the scaling of $\text{Im}F(s, t)/\text{Im}F(s, 0)$ with $\phi(\tau)$ being an entire function of order half. The crucial new result is the formula (13) for $\text{Re}F(s, t)$. In turn, this yields for the partial waves of $F^{(2)}$, if $b^2 \text{Im}a^{(2)}(b, s) \rightarrow 0$ for $b \rightarrow \infty$,

$$\text{Re } a^{(2)}(b, s) \rightarrow \frac{-\pi}{2 \ln(s/s_0)} b \frac{\partial}{\partial b} \text{Im } a^{(2)}(b, s), \quad s \rightarrow \infty. \quad (16)$$

However, in view of the slow approach to asymptotics, the formula (15) for $\text{Re}a(b, s)$ involving derivative over $\ln s$ is preferable for computations, as it holds also for $F^{(1)} + F^{(2)}$.

4.3. The total amplitude

Consistent with (13) for $\gamma = \beta = 2$, i.e. $\tau = t(\ln |s/s_0|)^2$, I adopt the ansatz,

$$\frac{\text{Re}F^{(2)}(s, t)}{\text{Im}F^{(2)}(s, 0)} = \frac{\pi}{\ln(s/s_0)} \frac{d}{d\tau} \left(\tau \frac{\text{Im}F^{(2)}(s, t)}{\text{Im}F^{(2)}(s, 0)} \right). \quad (17)$$

For simplicity, I choose the scale factor s_0 to be the same as in the PDG (2005) [3] fit for pp total cross section, $\sqrt{s_0} = 5.38$ GeV. Substituting the expression for $\text{Im}F^{(2)}(s, t)$ I obtain,

$$\begin{aligned} \frac{16\pi}{k\sqrt{s}} F^{(2)}(s, t) &= \sigma_{\text{tot}}^{(2)}(s) \left[\frac{\pi}{\ln(s/s_0)} \right. \\ &\times \left. \frac{8J_2(qR(s)) - 16J_4(qR(s))}{q^2 R^2(s)} + i \frac{48J_3(qR(s))}{(qR(s))^3} \right]. \end{aligned} \quad (18)$$

The total amplitude $F(s, t) = F^{(1)}(s, t) + F^{(2)}(s, t)$ is now completely specified (analytically) by adding $F^{(1)}(s, t)$ given by (7). The important parameter $R^2(s)$ is determined from the experimental slope parameter $B(s) = (d/dt)(\ln d\sigma/dt)|_{t=0}$, if the Pomeron parameters b_P, α' are known,

$$\begin{aligned} R^2(s) (\epsilon(s) \sigma_{\text{tot}}^{(2)}(s)^2 + \frac{1}{2} \sigma_{\text{tot}}^{(2)}(s) \sigma_{\text{tot}}(s)) \\ = 4B(s) (\epsilon(s) \sigma_{\text{tot}}^{(2)}(s)^2 + \sigma_{\text{tot}}(s)^2) \\ - \sigma_{\text{tot}}^{(1)}(s) D^2(s) - 4\pi \alpha' \sqrt{\epsilon(s)} \sigma_{\text{tot}}^{(1)}(s) \sigma_{\text{tot}}^{(2)}(s), \end{aligned} \quad (19)$$

where, we denote $\sqrt{\epsilon(s)} \equiv \pi/\ln(s/s_0)$. For the experimental slope parameter I shall use the fits $B(M, s)$ to all pp data, with $M = 1, 2$, $B(1, s)$ by Okorokov [6] and $B(2, s)$ by Schegelsky–Ryskin [5],

$$\begin{aligned} B(1, s) &= 8.81 + 0.396 \ln s + 0.013 (\ln s)^2 \text{ GeV}^{-2}, \\ B(2, s) &= 11.03 + 0.0286 (\ln s)^2 \text{ GeV}^{-2}, \end{aligned} \quad (20)$$

where \sqrt{s} is in GeV units. For $pp, \bar{p}p$ total cross sections I use the PDG fits of (2005) and (2013),

$$\begin{aligned} \sigma_{\text{tot}}^{(2005)}(s) &= 35.63 + 0.308 \left(\ln \left(\frac{s}{28.94} \right) \right)^2 \text{ mb} \\ \sigma_{\text{tot}}^{(2013)}(s) &= 33.73 + 0.2838 \left(\ln \left(\frac{s}{15.618} \right) \right)^2 \text{ mb}. \end{aligned} \quad (21)$$

4.4. Elastic and inelastic cross sections

The integrals over impact parameter needed to calculate σ_{el} can be done exactly. We obtain,

$$\begin{aligned} \sigma_{el}(s) &= (\pi/2) C^2(s) D^2(s) (2 + (\beta'(s))^2) \\ &+ 4\pi R^2(s) E^2(s) (3 + 2\epsilon(s))/15 \\ &+ 2\pi R^2(s) C(s) E(s) \delta^{-3}(s) \left[\exp(-2\delta(s)) \right. \\ &\times (-1 + 2\beta'(s)\sqrt{\epsilon(s)}) (2\delta^2(s) + 3\delta(s) + 2) + \\ &\left. (2\beta'(s)\sqrt{\epsilon(s)}(\delta(s) - 2) + 2\delta^2(s) - 2\delta(s) + 1) \right], \\ \delta(s) &\equiv R^2(s)/D^2(s), \quad \beta'(s) \equiv 4\pi \alpha'/D^2(s). \end{aligned} \quad (22)$$

5. Predictions of the model versus experimental data for pp and $\bar{p}p$ scattering

5.1. Differential cross sections

Remarkably, a single pair of values of the Pomeron parameters b_P, α' ,

$$b_P = 3.8 \text{ GeV}^{-2}, \quad \alpha' = 0.07 \text{ GeV}^{-2}, \quad (23)$$

gives very good agreement of model predictions in the entire range $|t| < 0.3 \text{ GeV}^2$ with the experimental Totem [7–10] and Atlas [12–15] pp differential cross sections at 7 TeV and 8 TeV, experimental $\bar{p}p$ differential cross sections at 546 GeV from UA4 collaborations, D. Bernard et al. [44] and M. Bozzo et al. [45], and at 1800 GeV from Amos et al. [46] and Abe et al. [47]. (See also the compilation in [48].) This agreement is independent of the choice between PDG (2005) and PDG (2013) total cross sections, and the choice between slopes $B(1, s)$ and $B(2, s)$. We exhibit this in Figs. 1, 2, 3, 4 for forward slope choice $B = B(2, s)$ [5] and the two choices of total cross sections PDG (2005) [3] (dashed curve), and PDG (2013) [4] (solid curve). (Differential cross sections for $(-t) > 0.3 \text{ GeV}^2$ are not used in determination of Pomeron parameters b_P, α' as they make negligible contributions to σ_{el} in this energy range; e.g. in this model, about 0.2 mb at 7 TeV and 8 TeV.)

For the choice $B = B(2, s)$ [5] and PDG (2013) [4] total cross sections, we give below three parameter fits to predicted differential cross sections in this range of t at c.m. energies upto 14 TeV,

$$\begin{aligned} \ln((d\sigma/dt)/(d\sigma/dt)_{t=0}) &= 19.5t - 11.9t^2 + 43.5(-t)^3, \quad 7 \text{ TeV} \\ &= 19.7t - 13.2t^2 + 47.3(-t)^3, \quad 8 \text{ TeV} \\ &= 20.5t - 19.2t^2 + 64.2(-t)^3, \quad 13 \text{ TeV} \\ &= 20.6t - 20.3t^2 + 67.2(-t)^3, \quad 14 \text{ TeV} \end{aligned} \quad (24)$$

for ready comparisons with existing and future data.

5.2. Inelastic cross sections

Fig. 5 depicts the predicted inelastic cross sections up to 100 TeV and their asymptotic fits. Tables 1 and 2 give model parameters and detailed predictions from 546 GeV to 14 TeV, with input total cross sections PDG2013 and PDG2005 respectively. The predicted $\rho = \text{Re}F(s, t)/\text{Im}F(s, t)|_{t=0}$ and the predicted inelastic cross sections (e.g. for input total cross section PDG2013, $\rho = 0.136$, $\sigma_{inel} = 74.2$ mb, at 8 TeV) are very close to available experimental values [49,50,7–10,12–15]. The predicted inelastic cross sections are fairly robust, changing by less than 0.5 mb in the range (7 TeV, 14 TeV) when the slope parameter is changed from $B(1, s)$ to $B(2, s)$ and by less than 1 mb when the input σ_{tot} is changed from PDG (2005) to PDG (2013). Model results give $\partial\sigma_{inel}/\partial B \sim 1.07 \text{ mb GeV}^2$, $\partial\sigma_{inel}/\partial\sigma_{tot} \sim 0.46$, and using input errors of PDG2013 fits, and $\delta B \sim 0.3 \text{ GeV}^{-2}$ upto 100 TeV [5], I have the error estimate, $\delta\sigma_{inel} \sim .47 + .0021 (\ln(s/15.618))^2 \text{ mb}$.

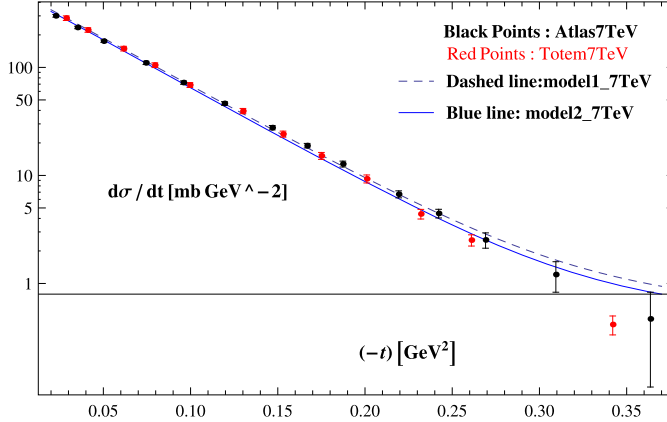


Fig. 1. Model predictions for pp elastic differential cross sections $d\sigma/dt$ at 7 TeV, with parameters $b_P = 3.8 \text{ GeV}^{-2}$, $\alpha' = 0.07 \text{ GeV}^{-2}$, forward slope from Schegelsky-Ryskin fit [5], input σ_{tot} from PDG (2005) [3] (dashed curve), and input σ_{tot} from PDG (2013) [4] (solid curve), show excellent agreement with experimental values from the Totem [7–10] and Atlas [12–15] collaborations for $|t| < 0.3 \text{ GeV}^2$.

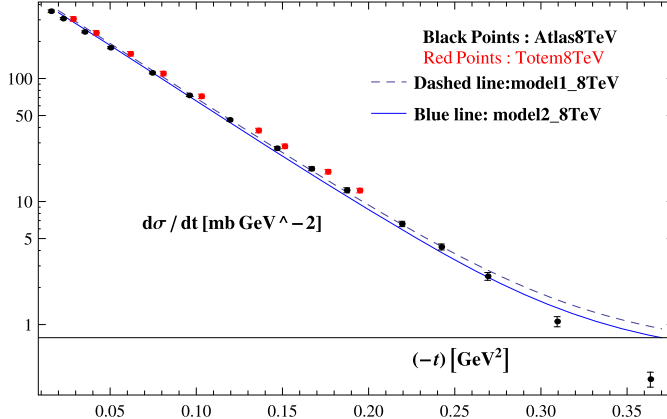


Fig. 2. Model predictions for pp elastic differential cross sections $d\sigma/dt$ at 8 TeV, with parameters $b_P = 3.8 \text{ GeV}^{-2}$, $\alpha' = 0.07 \text{ GeV}^{-2}$, forward slope from Schegelsky-Ryskin fit [5], input σ_{tot} from PDG (2005) [3] (dashed curve), and input σ_{tot} from PDG (2013) [4] (solid curve), show excellent agreement with experimental values from the Totem [7–10] and Atlas [12–15] collaborations for $|t| < 0.3 \text{ GeV}^2$.

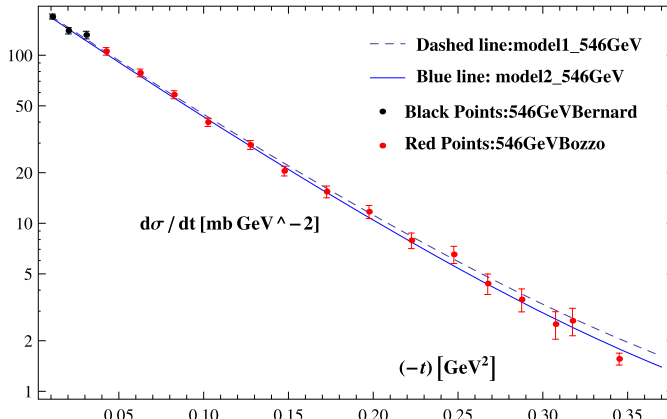


Fig. 3. Model predictions for $\bar{p}p$ elastic differential cross sections $d\sigma/dt$ at 546 GeV, with parameters $b_P = 3.8 \text{ GeV}^{-2}$, $\alpha' = 0.07 \text{ GeV}^{-2}$, forward slope from Schegelsky-Ryskin fit [5], input σ_{tot} from PDG (2005) [3] (dashed curve), and input σ_{tot} from PDG (2013) [4] (solid curve), show good agreement with experimental values from UA4 collaborations, D. Bernad et al. [44] and M. Bozzo et al. [45] for $|t| < 0.3 \text{ GeV}^2$.

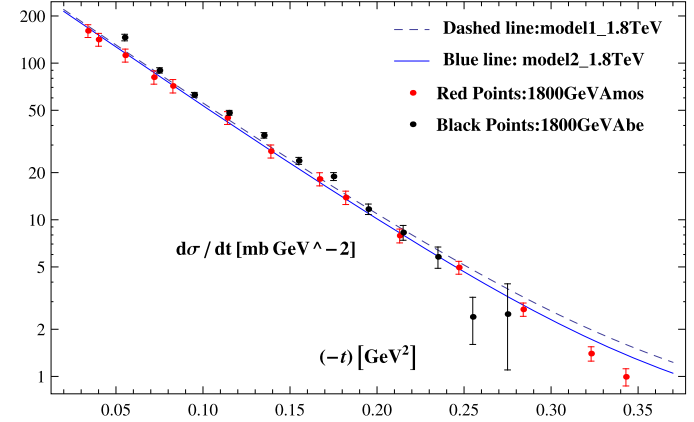


Fig. 4. Model predictions for $\bar{p}p$ elastic differential cross sections $d\sigma/dt$ at 1800 GeV, with parameters $b_P = 3.8 \text{ GeV}^{-2}$, $\alpha' = 0.07 \text{ GeV}^{-2}$, forward slope from Schegelsky-Ryskin fit [5], input σ_{tot} from PDG (2005) [3] (dashed curve), and input σ_{tot} from PDG (2013) [4] (solid curve), show good agreement with experimental values from Amos et al. [46] and Abe et al. [47] for $|t| < 0.3 \text{ GeV}^2$.

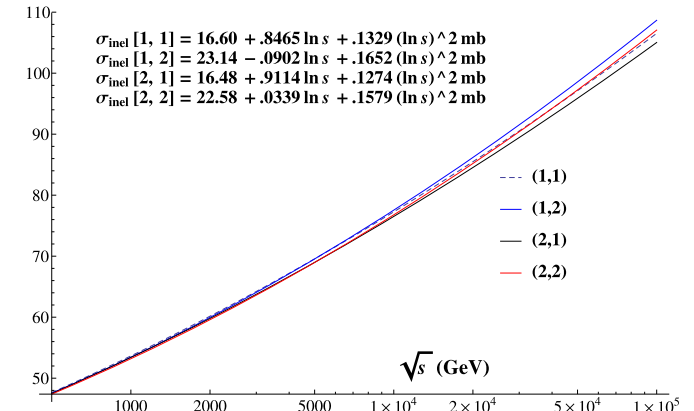


Fig. 5. Plots of pp inelastic cross sections $\sigma_{inel}(q, M)$ computed from the model with $q = 1$ and $q = 2$ signifying inputs of σ_{total} (PDG – 2005) [3] and σ_{total} (PDG – 2013) [4] respectively and $M = 1$ and $M = 2$ signifying inputs of Okorokov [6] and Schegelsky-Ryskin [5] slopes respectively. Input Pomeron parameters are $b_P = 3.8 \text{ GeV}^{-2}$, $\alpha' = 0.07 \text{ GeV}^{-2}$. Three parameter fits to these inelastic cross sections are also shown.

In the c.m. energy range from 0.5 TeV to 100 TeV, the model parameters are very well approximated by the following fits.

Input $\sigma_{tot}^{(2005)}(s)$:

$$\begin{aligned}M = 1 : E(s) &= 0.987849 - 20.3797/x + 113.797/x^2 \\ M = 1 : R^2(s) &= 241.078 - 9.20435x + 0.375387x^2 \\ M = 2 : E(s) &= 0.861023 - 16.7296/x + 88.3041/x^2 \\ M = 2 : R^2(s) &= 245.408 - 11.3716x + 0.487702x^2\end{aligned}\quad (25)$$

Input $\sigma_{tot}^{(2013)}(s)$:

$$\begin{aligned}M = 1 : E(s) &= 0.936736 - 18.91/x + 104.505/x^2 \\ M = 1 : R^2(s) &= 214.735 - 6.85598x + 0.320973x^2 \\ M = 2 : E(s) &= 0.812299 - 15.3352/x + 79.6064/x^2 \\ M = 2 : R^2(s) &= 220.921 - 9.20272x + 0.437436x^2\end{aligned}\quad (26)$$

where, $x \equiv \ln s$.

Remarkably, fits for input $\sigma_{tot}^{(2005)}(s)$ show that the choice $M = 1$ gives $E(s)$ which is barely below the unitarity limit for $s \rightarrow \infty$. The inelastic cross section fits in Fig. 5 yield,

Table 1

Detailed results at 546 GeV, 1.8 TeV, 7 TeV, 8 TeV, 13 TeV and 14 TeV from the model using inputs $b_p = 3.8$, $\alpha' = .07 \text{ GeV}^{-2}$, PDG 2013 values of $\sigma_{\text{tot}}(pp)$ [4], and Schegelsky–Ryskin extrapolations ($M = 2$, i.e. $B = B(2, s)$) [5] for forward slopes. The output parameters C and E show explicitly that inelastic unitarity is obeyed. The output values of R^2 show a slowly expanding size of the proton with increasing energy. The output results for $\sigma_{\text{inel}}/\sigma_{\text{tot}}$, $16\pi\sigma_{\text{el}}B/\sigma_{\text{tot}}^2$, and $\rho = \text{Re}F(s, t=0)/\text{Im}F(s, t=0)$, which would be $1/2$, 1 and 0 respectively in the black disk limit, give quantitative measures for deviations from that limit. The output ρ agrees with available experiments [49,50]. The output values of σ_{inel} agree within errors with Totem results [7–10] and Atlas results [12–15] for pp scattering at 7 TeV and 8 TeV, and with the results of [47] for $\bar{p}p$ scattering at 546 GeV and 1800 GeV. Model predictions at higher energies can be tested in future experiments.

M=	2	2	2	2	2	2
$\sqrt{s} (\text{GeV})$	546	1800	7000	8000	13 000	14 000
$\sigma_{\text{tot}} (\text{mb})$ PDG2013	61.303	76.2666	97.2354	99.5232	108.183	109.551
$D^2 (\text{GeV}^{-2})$	37.4589	38.795	40.3161	40.4657	41.0094	41.0924
$B (\text{GeV}^{-2})$	15.5743	17.4574	19.9975	20.2701	21.2954	21.4566
C	0.368032	0.355357	0.341949	0.340686	0.336168	0.335489
E	0.0967198	0.144442	0.199302	0.2046	0.223619	0.226485
$R^2 (\text{GeV}^{-2})$	174.777	180.545	195.35	197.148	204.121	205.243
$\sigma_{\text{inel}}/\sigma_{\text{tot}}$	0.784689	0.767591	0.747523	0.745582	0.738615	0.737567
$16\pi\sigma_{\text{el}}B/\sigma_{\text{tot}}^2$	1.07068	1.04127	1.01634	1.01425	1.0071	1.00607
ρ	0.143356	0.143121	0.137163	0.136402	0.133487	0.133025
$\sigma_{\text{inel}} (\text{mb})$	48.1038	58.5415	72.6858	74.2027	79.9053	80.8015

Table 2

Same as Table 1, but for input σ_{tot} (PDG-2005). Comparison shows that the predicted inelastic cross section at 7 TeV (8 TeV) increases by about 0.7 mb, when the input σ_{tot} increases by 1.8 mb (1.9 mb).

M=	2	2	2	2	2	2
$\sqrt{s} (\text{GeV})$	546	1800	7000	8000	13 000	14 000
$\sigma_{\text{tot}} (\text{mb})$ PDG2005	61.9255	77.2584	98.983	101.364	110.393	111.822
$D^2 (\text{GeV}^{-2})$	37.4589	38.795	40.3161	40.4657	41.0094	41.0924
$B (\text{GeV}^{-2})$	15.5743	17.4574	19.9975	20.2701	21.2954	21.4566
C	0.388763	0.375374	0.361211	0.359876	0.355105	0.354387
E	0.0895596	0.138997	0.196895	0.20253	0.222814	0.225877
$R^2 (\text{GeV}^{-2})$	180.005	183.611	197.264	198.984	205.713	206.802
$\sigma_{\text{inel}}/\sigma_{\text{tot}}$	0.779607	0.762221	0.741121	0.739053	0.731598	0.730472
$16\pi\sigma_{\text{el}}B/\sigma_{\text{tot}}^2$	1.08493	1.05165	1.02371	1.02138	1.01343	1.01228
ρ	0.144376	0.145604	0.1402	0.139456	0.136561	0.136098
$\sigma_{\text{inel}} (\text{mb})$	48.2776	58.888	73.3584	74.9136	80.7634	81.6831

Input $\sigma_{\text{tot}}^{(2013)}(s) :$

$$M = 1 : \frac{\sigma_{\text{inel}}}{\sigma_{\text{tot}}} \rightarrow 0.449; M = 2 : \frac{\sigma_{\text{inel}}}{\sigma_{\text{tot}}} \rightarrow 0.556$$

Input $\sigma_{\text{tot}}^{(2005)}(s) :$

$$M = 1 : \frac{\sigma_{\text{inel}}}{\sigma_{\text{tot}}} \rightarrow 0.431; M = 2 : \frac{\sigma_{\text{inel}}}{\sigma_{\text{tot}}} \rightarrow 0.536 \quad (27)$$

These results are close to the black disk value of $1/2$ favoured by BH [39,40]. Recent detailed analysis of high energy data [51] concluded that, although consistent with experimental data, the black disk does not represent an unique solution.

5.3. Phenomenological lowest t -channel singularity

If continued to complex t , $|F(s, t)|$ given by this model is bounded by $\text{Const.}s^2$ for $s \rightarrow \infty$ and

$$|t| < t_1 = \min[(1/\alpha'), \lim_{s \rightarrow \infty} (\ln s/R(s))^2]. \quad (28)$$

Jin and Martin [52] proved that for $|t| < t_0$, where t_0 is the lowest t -channel singularity, twice subtracted dispersion relations in s hold. Hence t_1 may be thought of as a phenomenological lowest t -channel singularity. Using the formulae for $R^2(s)$ given above,

Input $\sigma_{\text{tot}}^{(2013)}(s) :$

$$M = 1 : \sqrt{t_1} = 1.765 \text{ GeV}; M = 2 : \sqrt{t_1} = 1.512 \text{ GeV};$$

Input $\sigma_{\text{tot}}^{(2005)}(s) :$

$$M = 1 : \sqrt{t_1} = 1.632 \text{ GeV}; M = 2 : \sqrt{t_1} = 1.432 \text{ GeV}.$$

Our $\sqrt{t_1} \sim 1.4\text{--}1.8$ GeV is reminiscent of, but different from the glue-ball mass of BH [39,40]. Given the instability of analytic continuations, its main function is to suggest that the usual Lukaszuk–Martin bound [20] is quantitatively poor as it assumes lack of t -channel singularities only upto $4m_\pi^2$ which is much smaller than t_1 .

6. Conclusion

I presented an analytic formula for the high energy elastic amplitude $F(s, t) = F^{(1)}(s, t) + F^{(2)}(s, t)$ given by Eqs. (7), (18) for $\sqrt{s} > 100$ GeV, exhibiting Froissart bound saturation, AKM scaling [1,2], inelastic unitarity, predicting differential cross sections for $(-t) < 0.3 \text{ GeV}^2$ and total inelastic cross sections, at 546 GeV, 1800 GeV, 7 TeV and 8 TeV in agreement with experimental results, as well as the real parts and inelastic cross sections upto 100 TeV. An ‘effective’ t -channel singularity at $\sqrt{t} \sim 1.4\text{--}1.8$ GeV is suggested by analytic continuation to positive t . Detailed tables and graphs of model parameters, real parts and cross sections upto 100 TeV will be published separately. The ‘grey disk’ component could be generalized using a smoother impact parameter cut-off, i.e. $n > 1$ in Eq. (5).

Acknowledgements

I presented an earlier version with a black disk second component in 2015 to André Martin and T.T. Wu at CERN; their insistence that a sharp impact parameter cut-off is too ‘brutal’ led to the black disk being replaced by the grey disk. I thank G. Auberson for remarks concerning instability of analytic continuation, D. Atkinson, G. Mahoux and V. Singh for helpful comments on the manuscript; I also thank Gilberto Colangelo and Heiri Leutwyler for very helpful discussions, and a seminar invitation at Univ. of Bern, and Irinel Caprini and Juerg Gasser for discussions on a very stimulating ansatz for high energy pion-pion scattering [53]. I thank the referees for the crucial suggestion of comparison with the latest differential cross section data and the Indian National Science Academy for an INSA senior scientist grant.

References

- [1] G. Auberson, T. Kinoshita, A. Martin, Phys. Rev. D 3 (1971) 3185.
- [2] G. Auberson, S.M. Roy, Nucl. Phys. B 117 (1976) 322.
- [3] S. Eidelman, et al., Particle data Group, Phys. Lett. B 592 (2004) 1, and 2005 partial update, Table 40.2, <http://pdg.lbl.gov/2005>.
- [4] J. Beringer, et al., Particle data Group, Phys. Rev. D 86 (2012) 010001, and 2013 partial update, Table 50, <http://pdg.lbl.gov/2013>.
- [5] V.A. Schegelsky, M.G. Ryskin, Phys. Rev. D 85 (2012) 094024.
- [6] V.A. Okorokov, arXiv:1501.01142v2 [hep-ph], 23 May 2015.
- [7] Totem Collaboration, G. Antchev, et al., Europhys. Lett. 96 (2011) 21002.
- [8] Totem Collaboration, G. Antchev, et al., Europhys. Lett. 101 (21004) (2013), CERN-PH-EP-2012-239.
- [9] Totem Collaboration, G. Antchev, et al., Phys. Rev. Lett. 111 (2013) 012001.
- [10] Totem Collaboration, G. Antchev, et al., Nucl. Phys. B 899 (2015) 527, arXiv:1503.08111 [hep-ex].
- [11] CMS Collaboration, Phys. Lett. B 722 (2013) 5, presentation at EPS-HEP Conference, Vienna, 22–29 July, 2015.
- [12] Atlas Collaboration, Nat. Commun. 2 (2011) 463.
- [13] Atlas Collaboration, Nucl. Phys. B 889 (2014) 486, arXiv:1408.5778v2 [hep-ex].
- [14] Atlas Collaboration, ATLAS-CONF-2015-038.
- [15] Atlas Collaboration, Phys. Lett. B (2016), submitted for publication, CERN-EP-2016-158, 25 July 2016, arXiv:1607.06605v1 [hep-ex].
- [16] Alice Collaboration, arXiv:1208.4968, 2012.
- [17] Pierre Auger Collaboration, Phys. Rev. Lett. 109 (2012) 062002.
- [18] M. Froissart, Phys. Rev. 123 (1961) 1053.
- [19] A. Martin, Nuovo Cimento 42 (1966) 930.
- [20] L. Lukaszuk, A. Martin, Nuovo Cimento A 52 (1967) 122.
- [21] S.M. Roy, Phys. Rep. 5C (1972) 125.
- [22] J. Kupsch, Nuovo Cimento A 71 (1982) 85.
- [23] H. Cheng, T.T. Wu, Phys. Rev. Lett. 24 (1970) 1456.
- [24] C. Bourrely, J. Soffer, T.T. Wu, Phys. Rev. D 19 (1979) 3249.
- [25] C. Bourrely, J. Soffer, T.T. Wu, Nucl. Phys. B 247 (1984) 15.
- [26] C. Bourrely, J. Soffer, T.T. Wu, Z. Phys. C 37 (1988) 369.
- [27] C. Bourrely, J. Soffer, T.T. Wu, Eur. Phys. J. C 28 (2003) 97.
- [28] C. Bourrely, J. Soffer, T.T. Wu, Eur. Phys. J. C 71 (2011) 1061.
- [29] M.M. Block, et al., Phys. Rev. D 60 (1999) 054024.
- [30] M.M. Block, Phys. Rep. 436 (2006) 71.
- [31] M.M. Block, F. Halzen, Phys. Rev. D 83 (2011) 077901.
- [32] M.M. Islam, et al., Int. J. Mod. Phys. A 21 (2006) 1.
- [33] A. Martin, Phys. Rev. D 80 (2009) 065013.
- [34] T.T. Wu, A. Martin, S.M. Roy, V. Singh, Phys. Rev. D 84 (2011) 025012.
- [35] A. Martin, S.M. Roy, Phys. Rev. D 89 (2014) 045015.
- [36] A. Martin, S.M. Roy, Phys. Rev. D 91 (2015) 076006.
- [37] R.F. Avila, P. Gauron, B. Nicolescu, Eur. Phys. J. C 49 (2007) 581.
- [38] E. Martynov, B. Nicolescu, Eur. Phys. J. C 56 (2008) 57.
- [39] M.M. Block, F. Halzen, Phys. Rev. Lett. 107 (2011) 212002.
- [40] Phys. Rev. D 86 (2012) 051504(R).
- [41] N.N. Khuri, T. Kinoshita, Phys. Rev. B 137 (1965) 720.
- [42] A. Martin, Lett. Nuovo Cimento 7 (1973) 811.
- [43] A. Martin, CERN-TH/97-23, 1997.
- [44] D. Bernard, et al., UA4 Collaboration, Phys. Lett. B 198 (1987) 583.
- [45] M. Bozzo, et al., UA4 Collaboration, Phys. Lett. B 147 (1984) 385.
- [46] N.A. Amos, et al., Phys. Lett. B 247 (1990) 127.
- [47] F. Abe, et al., Phys. Rev. D 50 (1994) 5518, Phys. Rev. D 50 (1994) 5550.
- [48] J.R. Cudell, A. Lengyel, E. Martynov, Phys. Rev. D 73 (034008) (2006), arXiv:hep-ph/0511073.
- [49] COMPETE Collaboration, J.R. Cudell, et al., Phys. Rev. Lett. 89 (2002) 201801.
- [50] COMPETE Collaboration, J.R. Cudell, et al., Phys. Rev. D 65 (2002) 074024.
- [51] D.A. Fagundes, M.J. Menon, P.V.R.G. Silva, Nucl. Phys. A 946 (2016) 194.
- [52] Y.S. Jin, A. Martin, Phys. Rev. 135B (1964) 1375.
- [53] I. Caprini, G. Colangelo, H. Leutwyler, Eur. Phys. J. C 72 (2012) 1860.